Chemical Science

Accepted Manuscript

This article can be cited before page numbers have been issued, to do this please use: T. Wang, D. Chen, X. Li, H. Wang, J. Li, L. Hao, Y. Fang, S. Yu, L. Zhao, S. Chen, Y. Ning, Y. Meng, J. Hu and T. Liu, *Chem. Sci.*, 2026, DOI: 10.1039/D6SC01713D.

ROYAL SOCIETY OF CHEMISTRY

rsc.li/chemical-science

View Article Online
DOI: 10.1039/D6SC01713D

ARTICLE

Engineering Covalent Organic Frameworks for Decoupled Photocatalytic and Dark Photocatalytic Synthesis of H_2O_2

Received 00th January 20xx,
Accepted 00th January 20xx

DOI: 10.1039/x0xx00000x

Tian Wang[a], Du-Yong Chen[a], Xin-Feng Li[a], Hao Wang[a], Jing Li[a], Lu-Lu Hao[a], Yan Fang[a], Yu Shan[a], Liang Zhao[a], Shu-Xin Chen[d], Yingying Ning[d], Yin-Shan Meng*[a, c], Jiyun Hu*[b], and Tao Liu*[a, c]

Mimicking both the photo reaction and dark reaction units in the natural photosynthetic system offers a sustainable approach for the efficient capture and storage of solar energy. Here we demonstrate that an engineered quinoline-linked covalent organic framework (Py-1Q) can integrate electron transport and storage within a single material. Under visible light illumination, Py-1Q exhibits a H_2O_2 production rate of 1535 μmol g^{-1} h^{-1}, 8.5 times higher than that of its imine counterpart. Moreover, part of the photo energy was stored in Py-1Q as free electrons during irradiation, which can be gradually released in the dark to further produce 95 μmol g^{-1} h^{-1} of H_2O_2. DFT calculations reveal that the enhanced delocalization of the lowest unoccupied molecular orbital of Py-1Q is critical for its charge storage property. This study expands the applications of functional COFs and offers new insights into the design of solar-energy storage materials.

Introduction

Artificial photosynthesis represents a sustainable solution to the energy and environment crisis our society is facing, yet poses great challenges to our current solar utilization technologies. The high efficiency of the natural photosynthetic system hinges on the cooperation of multiple cofactors, including the crucial light-dependent reactions (photosystem II and I, namely PSII and PSI) and the light-independent dark reactions (Calvin cycle).[1] PSII and PSI absorb photon energy to form charge separation states, which drive water oxidation to release oxygen, electrons, and protons.[2,3] Then the proton/electron separated energy is stored in nicotinamide adenine dinucleotide phosphate (NADPH) and adenosine triphosphate (ATP), which are used to fix atmospheric CO_2 into carbohydrates in the Calvin cycle.[4,5] Inspired by the natural process, artificial photosynthesis has particularly advanced in the design of light reaction systems in recent years, achieving diverse photocatalytic transformations in a plug-and-play fashion.[6-8] However, mimicking the dark reaction system that is capable of storing photogenerated charges and releasing them on demand, i.e., the dark photocatalysis process, remains far more challenging.[9]

In fact, a database of dark photocatalytically active materials recently curated by Savateev et al. has no more than 100 entries.[10] The prevailing charge storage mechanism relies on a one-electron reduction of redox-active metals, such as Ti,[11] Cu,[12] and W oxides[13, 14], in the presence of a hole scavenger. However, the poor light-harvesting properties of inorganic oxides lead to low photoenergy utilization efficiency. In this regard, organic or inorganic-organic hybrids become promising alternative candidates. A few examples of isolated metal centers in metal-organic frameworks (MOFs) showed similar electron storage ability via metal fragment reduction.[15-18] Besides, 2D polymeric ionic carbon nitrides were found to trap electrons at the C- or N-centered radicals, offering a new way to store photo-generated electrons.[19-22] Despite of the alleviated light absorption issue, these materials still suffer three main drawbacks: 1) an organic sacrificial electron donor (SED) as hole scavenger is needed to accumulate electrons in organic solutions; 2) the photo-charged state is extremely sensitive to oxygen with a short lifetime under ambient environment conditions; and 3) most of dark photocatalytic reaction is initiated only upon the introduction of an external metal catalyst, for example Pt for hydrogen evolution reaction (HER), thus ending the materials' charge storage ability simultaneously. Therefore, developing a single-component multifunctional

[a] State Key Laboratory of Fine Chemicals, Frontier Science Center for Smart Materials, School of Chemical Engineering, Dalian University of Technology, No.2 Linggong Road, Dalian 116024, China; E-mail: mengys@dlut.edu.cn; liutao@dlut.edu.cn.
[b] Dongguan Key Laboratory of Interdisciplinary Science for Advanced Materials and Large-Scale Scientific Facilities, School of Physical Sciences, Great Bay University, Dongguan 523000, China. E-mail: hujiyun@gbu.edu.cn
[c] Liaoning Binhai Laboratory, Dalian 116023, China
[d] Spin-X Institute, School of Chemistry and Chemical Engineering, School of Biomedical Sciences and Engineering, State Key Laboratory of Luminescent Materials and Devices, Guangdong-Hong Kong-Macao Joint Laboratory of Optoelectronic and Magnetic Functional Materials, South China University of Technology, Guangzhou 510641, China.
*Corresponding Author(s): Tao Liu: liutao@dlut.edu.cn; Jiyun Hu: hujiyun@gbu.edu.cn; Yin-Shan Meng: mengys@dlut.edu.cn

material that could fully mimic the natural photosynthesis process, i.e., operating in an aqueous atmospheric condition, is to be discovered.

To this end, we find that covalent organic frameworks (COFs) hold great potential to solve the aforementioned problems in dark photocatalysis.[23-26] COFs are crystalline conjugated polymers that have many merits for tailored applications.[27-32] Firstly, the framework designability at the molecular level allows one to fine-tune the band gap to match the oxidation potential of water when it is used as the hole scavenger. Secondly, the conjugated structure of COFs brings good visible light absorbing properties, and more importantly, potential electron storage capability.[33-38] On the other hand, finding a suitable reaction to store the chemical energy of photo-generated electrons in ambient conditions is equally important. The air sensitivity of the reported charged states suggests feasible electron transfer to O_2, yielding superoxide anion radical ($O_2^{\bullet-}$), which is an important intermediate in photocatalytic hydrogen peroxide (H_2O_2) synthesis.[39, 40] Combining the generated protons during photo-charging, the activation and conversion of O_2 to H_2O_2 as an energy carrier seems to be the ideal reaction. COFs as metal-free H_2O_2 synthesis photocatalysts have made great progress over the past years.[41] A key challenge is to rationally design a single-component system that can simultaneously facilitate spatial separation of photogenerated electron-hole pairs and stabilize the electrons after hole consumption.

In this work, we introduced a quinoline unit to engineer the frontier orbitals of a pyrene-based COF, leading to the desired functions for decoupled photo-dark catalysis. The quinoline COF Py-1Q demonstrated a moderate H_2O_2 production rate of 1535 μmol g^{-1} h^{-1} under visible light[42, 43] and more importantly a sustained rate of 95 μmol g^{-1} h^{-1} after light source removal. The slowly released electrons stored in Py-1Q continued to drive the production of H_2O_2 in the dark. The charge storage capacity was estimated to be 277 C g^{-1}, surpassing reported MOF systems. This study demonstrates that COFs can serve as efficient single-component charge storage media for light–dark decoupled catalysis, offering a novel design paradigm for sustainable energy storage and programmable chemical synthesis.

Results And Discussion

Synthesis and characterizations

Pyrene, a prominent electron-rich component with large π-conjugation and broad light absorption, has been widely used to construct photoactive COFs.[44, 45] We used Py-1P COF as a starting point, and a post-synthetic modification step was applied to transform the imine to quinoline linkage (Figure 1a, see supporting information for details).[46-48] In the presence of $Cu(OTf)_2$ catalyst, the imine linkage of Py-1P reacts with styrene oxide to form a quinoline linkage. This transformation increases the conjugation of the whole framework, laying the foundation for stabilizing photo-generated electrons. Multiple spectroscopic techniques verified the successful linkage transformation. In the FT-IR spectra of Py-1Q COF, three new absorption bands at 1662, 1517, and 1250 cm^{-1} were observed, which are attributed to the quinoline ring stretching vibrations (Figure 1b). Additionally, the C=N stretching signal of the imine group in Py-1P COF (originally at ~1620 cm^{-1}) exhibited a significant intensity reduction. In the solid-state ^{13}C NMR spectra, the characteristic carbon peak of C=N at 157 ppm in Py-

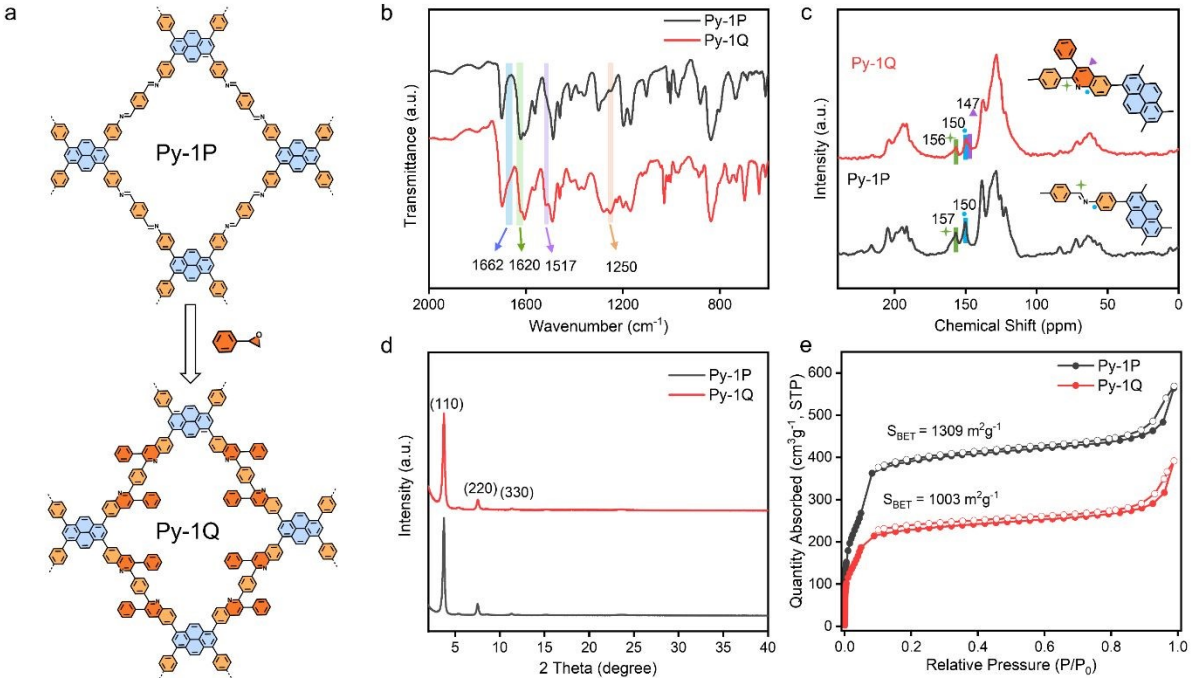

Figure 1. (a) Synthetic route of Py-1Q COF. (b) FT-IR spectra, (c) Solid-state ^{13}C NMR spectra (the peaks at 180-210 and 50-80 ppm are spinning sidebands), (d) PXRD patterns, and (e) N_2 sorption isotherms of Py-1P and Py-1Q.

View Article Online
DOI: 10.1039/D6SC01713D

1P COF shifted to 156 ppm in Py-1Q COF and a new peak at 147 ppm assigned to C4 of quinoline was observed (Figure 1c). X-ray photoelectron spectroscopy (XPS) measurements were also carried out to verify the chemical states of linked N atoms in these COFs. As shown in Figure S1, the peak of N 1s in Py-1P COF at 398.4 eV was slightly shifted to 398.3 eV in Py-1Q. These results collectively confirm the successful formation of the quinoline group in Py-1Q COF. Additionally, the Cu residue in Py-Q1 was determined to be 0.12 wt.% by inductively coupled plasma mass spectrometry (ICP-MS).

Powder X-ray diffraction (PXRD) analyses were employed to elucidate the crystalline structure of the synthesized COFs. Py-1Q COF showed a similar PXRD pattern to that of Py-1P COF (Figure 1d), implying preserved crystalline structure. The peaks at 3.76, 7.53, and 11.29° were assigned to (110), (220), and (330) facets, respectively, according to the simulated structure (Figure S2). The porosity of the COFs was studied using N_2 sorption at 77 K. Both COFs exhibited a type I isotherm (Figure 1e). The Brunauer–Emmett–Teller (BET) specific surface areas of Py-1P and Py-1Q were determined to be 1309 and 1003 $m^2 g^{-1}$, respectively. Pore sizes derived from non-local density function theory were 1.7 and 1.4 nm for Py-1P and Py-1Q, respectively, matching the simulated structures (Figure S3). The decrease in surface area and pore size corroborates the increased framework mass and reduced pore channel dimensions. Scanning electron microscopy (SEM) showed similar cubic aggregate morphology of Py-1P and Py-1Q. (Figure S4). To evaluate the chemical stability, Py-1P and Py-1Q were treated with 6 M HCl and 6 M NaOH at room temperature for 7 days. Under these harsh conditions, the imine-linked Py-1P COF was almost completely hydrolysed, with only 2 wt% solid residues recovered. In contrast, over 95 wt% of Py-1Q was retained. FT-IR spectroscopy confirmed the robustness of the quinoline linkage, and PXRD analysis showed only a slight peak intensity decrease, demonstrating the exceptional chemical stability of Py-1Q (Figure S5). The thermogravimetric analysis (TGA) also revealed that these COFs are thermally stable up to 350 ℃ under a nitrogen atmosphere (Figure S6).

Photophysical and electrochemical properties

To evaluate the light-harvesting capabilities of the COFs, the photophysical properties and electronic band structures of Py-1P and Py-1Q COFs were studied by UV-Vis diffuse reflectance spectroscopy (DRS) and Mott-Schottky measurements. As shown in Figure 2a, Py-1Q COF exhibited significantly broader absorption across the visible light spectrum compared to Py-1P COF, which is attributed to the enhanced π-conjugated structure. The optical band gaps of Py-1P and Py-1Q calculated from Tauc plots were determined to be 2.22 and 2.15 eV, respectively (Figure S7). Mott-Schottky measurements were performed to estimate the flat band potentials, with all COFs displaying characteristic n-type semiconductor behaviour. The flat band potentials versus Ag/AgCl (pH = 7) were determined as –0.82 and −0.89 V for Py-1P and Py-1Q, respectively (Figure 2b). The corresponding valence band edges were calculated to be 1.60 and 1.46 eV (*vs.* NHE), respectively. Furthermore, valence band maxima derived from valence band X-ray photoelectron spectroscopy are approximately 1.76 eV for Py-1P and 1.52 eV for Py-1Q (*vs.* NHE), in good agreement with the electrochemical results (Fig. S8). The increased conjugation of Py-1Q lowered both the conduction band and valence band positions compared to that of Py-1P. The band alignments of Py-1P and Py-1Q indicate that both COFs are thermodynamically feasible to drive oxygen reduction reaction (ORR) and water oxidation reaction (WOR, Figure 2c). A highly π-conjugated structure could facilitate charge separation and enhance the charge carrier lifetime. The photogenerated carrier migration efficiency of materials was evaluated through electrochemical, photoluminescence (PL) spectroscopy, and electron paramagnetic resonance (EPR) characterizations. The electrochemical impedance spectra (EIS, Figure S9) revealed that the quinoline-functionalized Py-1Q exhibited smaller semicircular Nyquist arc radii than Py-1P did, suggesting reduced charge transfer resistance. Upon light illumination, Py-1Q generated larger photocurrents than Py-1P, indicating promoted charge carriers (Figure 2d). The PL intensity of Py-1Q COF exhibited 91% decrease compared to that of Py-1P, indicating effectively suppressed electron-hole recombination (Figure 2e).[49, 50] This was also supported by the prolonged fluorescence lifetime of Py-1Q COF (0.37 ns) compared to that of Py-1P (0.22 ns, Figure 2f). To investigate the photoinduced free electron generation in COFs, we conducted electron paramagnetic resonance (EPR) measurements. Before light irradiation, both COFs displayed a single peak at g = 2.0023, mainly attributed to delocalized π-electrons within the framework (Figure S10).[51, 52] Py-1Q showed significantly stronger EPR signal intensity than Py-1P, highlighting the critical role of quinoline in enhancing π-electrons delocalization. Following 15 minutes of light exposure, Py-1Q showed a 3.3-fold enhancement of EPR signal intensity while Py-1P exhibited minimal EPR signal change. These observations demonstrate that Py-1Q is more efficient in promoting charge carrier generation and migration.

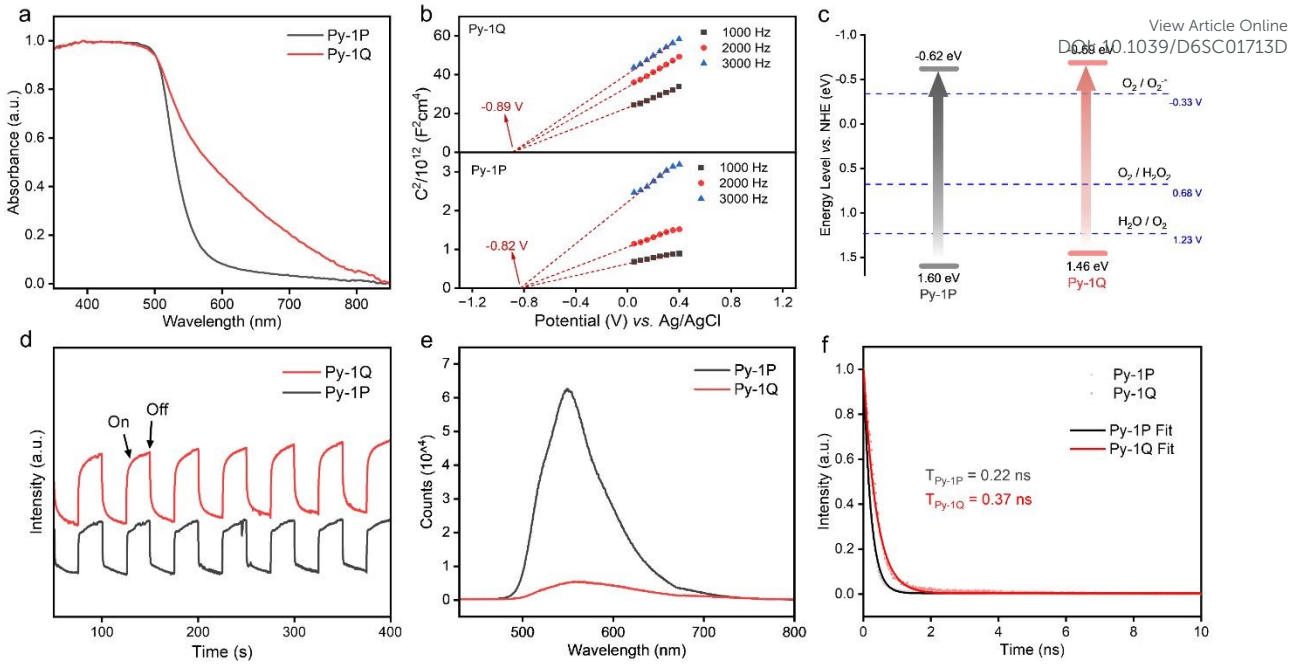

Figure 2. (a) UV-Vis diffuse reflectance spectra, (b) Mott-Schottky plots, (c) Energy level diagrams, (d) Transient photocurrent response measurements, (e) Steady-state photoluminescence spectra, and (f) Fluorescence decay profiles of Py-1P and Py-1Q.

Photocatalytic and dark photocatalytic synthesis of H_2O_2

As discussed before, the reduction of O_2 to H_2O_2 could serve as a model reaction for mimicking photocatalysis and dark photocatalysis. Both COFs were tested as heterogeneous catalysts for the synthesis of H_2O_2 under an air atmosphere. After 9 hours of light irradiation, the yield of H_2O_2 achieved 13816 μmol g^{-1} for Py-1Q, significantly higher than that of Py-1P (1621 μmol g^{-1}) by 8.5-fold (Figure 3a and S11). The enhanced photocatalytic performance of Py-1Q COF stems from the extended π-conjugated of the framework that promotes efficient charge separation. Interestingly, Py-1Q exhibited a gradual color change from orange to green during the reaction, indicating a charge storage process (Figure 3c).[49, 50] Py-1P maintained its orange color throughout the illumination period (Figure S12-13). Ex-situ UV-vis DRS measurements disclosed a distinct absorption band at 600-750 nm for Py-1Q after 9 h of illumination (Figure S14). The color of Py-1Q after light exposure could be partially recovered after 15 h in the dark, implying the release of the stored charge (Figure 3c). The corresponding UV-vis spectra showed the disappearance of the absorption band at 600-750 nm accordingly (Figure 3b). This reversible color change of Py-1Q from light irradiation and dark treatment is similar to that observed for those reported dark photocatalyst materials, suggesting electron storage during photo charging.[15, 17, 53] Indeed, methyl viologen, an electron acceptor, could reverse the color of photo charged Py-1Q from green to orange, supporting the electron storage proposal (Figure S15).[17] Monitoring the H_2O_2 concentration after removing the light source revealed an additional 1435 μmol g^{-1} production of H_2O_2 in 15 h, proving the dark photocatalytic capability of Py-1Q. The charge storage capacity was calculated to be 277 C g^{-1}, which exceeds reported MOF systems (Table S2). In contrast, Py-1P exhibited negligible H_2O_2 production under dark conditions (Figure 3a). However, the cycling performance is a bottleneck of Py-1Q. Significant performance decay in both photocatalysis and dark photocatalysis was observed. In the third cycle, the H_2O_2 yield under light and dark conditions dropped to ca. 25% and 20% of those in the first cycle, respectively (Figure S16).

View Article Online
DOI: 10.1039/D6SC01713D

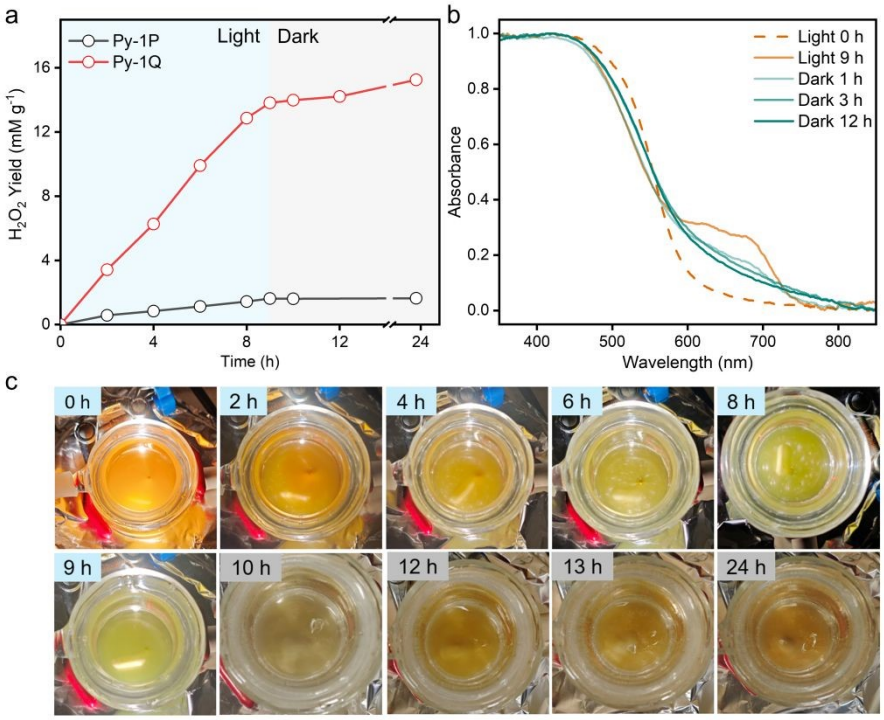

Figure 3. (a) Catalytic H_2O_2 production by Py-1P and Py-1Q with 300W Xe lamp irradiation (The data from three independent runs of catalysis and average yields of H_2O_2). (b) The DRS UV-Vis spectra of Py-1Q. (c) The color change of Py-1Q during the reaction (0-9 h, light; 10-24 h, dark).

The photocatalysis and dark photocatalysis mechanisms were investigated in more detail. First of all, the influence of Cu residue on the catalytic performance was studied. The introduction of additional $Cu(OTf)_2$ significantly reduced the yield of H_2O_2 in the photocatalysis period but did not affect the yield in the dark photocatalysis period (Figure S17). Assuming a Cu^+/Cu^{2+} electron storage mechanism, the Cu residue in Py-1Q accounts for a capacity of 1.8 C g^{-1}, much lower than the observed value. These results suggest that Cu is not involved in the charge storage process. A series of control and quenching experiments was then conducted to probe the reaction pathway. Under an argon atmosphere, the yield of H_2O_2 production dropped by 76% for Py-1Q, suggesting ORR as the major pathway (Figure 4a). The H_2O_2 production yield exhibited a marked 60% decrease upon the introduction of silver nitrate as an electron scavenger, implying the importance of photo-generated electrons in producing H_2O_2. A slight yield increase (11%) was observed when methanol was employed as a hole scavenger. Similar results were observed for Py-1P, suggesting the ORR as the main reaction pathway for H_2O_2 production (Figure 4a). Identification of the involvement of superoxide radicals ($O_2^{\bullet-}$) proved problematic using p-benzoquinone, which led to a dark substance that interferes with the quantification of H_2O_2 (Figure S18).

In order to explicitly probe the involved intermediates during H_2O_2 formation, we monitored the reaction using in-situ diffuse reflectance infrared Fourier transform (DRIFT) spectroscopy. The characteristic bands at 860 cm^{-1} (O-O stretching), 1180 cm^{-1} ($O_2^{\bullet-}$), and 2837 cm^{-1} (HOOH) steadily increase in intensity with the irradiation time, suggesting the two-step one-electron ORR pathway for both COFs (Figure 4b, 4c).[54, 55] Notably, under dark conditions, the peak intensities of the intermediates and H_2O_2 continued to increase for Py-1Q, while they remained nearly constant for Py-1P, demonstrating Py-1Q's dark photocatalysis ability.

Next, we used EPR spectroscopy to investigate the reaction mechanism. The aqueous suspension of Py-1P and Py-1Q under air conditions revealed distinct characteristics. Py-1P showed a negligible free radical signal at *g* of 2.0026 before light exposure, which could be slightly enhanced after 15 min of light exposure and degraded completely in 5 min in the dark afterwards (Figure 4d). On the other hand, Py-1Q showed a much stronger free radical signal at *g* of 2.0027 before light exposure, which was significantly enhanced after light exposure for 15 min. This free radical species exhibited slower degradation kinetics, which disappeared after 30 min in the dark (Figure 4g). This behavior proves that Py-1Q is more efficient than Py-1P in promoting photoelectron generation and preventing electron-hole recombination, consistent with its higher catalytic activity. The presence of photo-generated electrons was confirmed by trapping experiments with TEMPO. During 10 minutes of light irradiation, the EPR signal intensity of TEMPO decreased continuously in the presence of both COFs, demonstrating the accumulation of electrons (Figure 4e, h). To elucidate the fate of the photogenerated electrons and possible intermediates involved in the photocatalytic H_2O_2 synthesis, 5,5-dimethyl-1-pyrroline N-oxide (DMPO) was used as an $O_2^{\bullet-}$ trapping agent. As shown in Figures 4f and 4i, the characteristic signals for DMPO-$O_2^{\bullet-}$ were clearly detected in the presence of Py-1Q with significantly enhanced signal intensity compared to

View Article Online
DOI: 10.1039/D6SC04747D

that of Py-1P. More importantly, the DMPO-$O_2^{\bullet-}$ signal intensity for Py-1Q continued to increase even after the light illumination ceased and reached a plateau in 10 min (Figure 4i). This strongly indicates that electrons are stored in Py-1Q during irradiation, which can be released in dark conditions, consistent with its dark photocatalytic behavior in H_2O_2 synthesis. In contrast, the signal intensity for Py-1P decreased immediately after light was turned off (Figure 4f). These results are consistent with those obtained from in situ DRIFT studies.

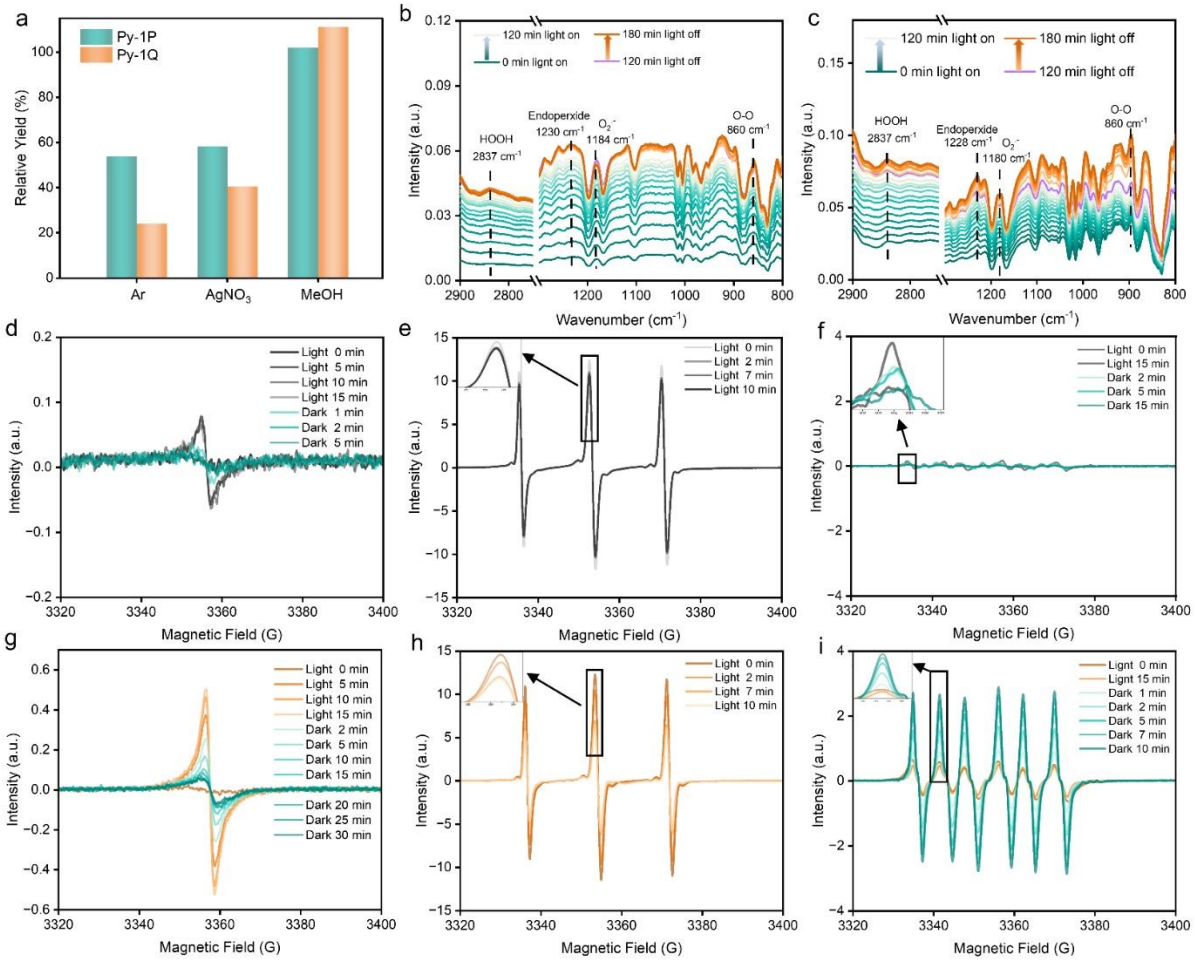

Figure 4. (a) The H_2O_2 production yields in the presence of different quenching agents relative to the corresponding standard conditions. In-situ DRIFTS spectra of Py-1P (b) and Py-1Q (c) during catalytic H_2O_2 production. EPR spectra of Py-1P (top panel) and Py-1Q (bottom panel) in H_2O (d, g), 1 mM TEMPO aqueous solution (e, h), and 100 mM DMPO methanol solution (f, i) under light and dark conditions, respectively.

Theoretical calculations

To understand the origin of the dark photocatalytic ability of Py-1Q, density functional theory (DFT) calculations were performed. The analysis of periodic electronic structure highlights the profound impact of quinoline incorporation on the frontier orbitals. In Py-1P, the HOMO is primarily localized on the pyrene core and the LUMO is confined to the adjacent imine linkages (Figure 5a). In Py-1Q, the HOMO is still mainly localized on the pyrene core, while the LUMO becomes extensively delocalized across the entire π-conjugated framework (Figure 5a). The delocalized LUMO could stabilize the photoinduced electrons and effectively suppresses electron–hole recombination, thereby enhancing both charge transport and storage.[56] Charge-transfer analysis further supports this conclusion. The calculated excited state charge migration from the electron-rich pyrene moiety to the quinoline linkage corresponds to transferred charges of 0.19 e^- for Py-1Q (Figure S20). In comparison, the number of transferred charges from pyrene to imine linkage for Py-1P is calculated to be 0.05 e^-. Moreover, band structure calculations confirm that Py-1Q possesses an indirect bandgap, which effectively suppresses radiative electron-hole recombination and prolongs charge carrier lifetimes (Figure S21).[57] The projected density of states (PDOS) analyses show that Py-1Q exhibits a broader and more continuous conduction band, implying more efficient electron excitation and relaxation processes (Figure S21). We have also calculated the charge storage state of Py-1Q by adding one extra electron per unit cell. The relaxed structure shows that the spin density is distributed over the conjugated framework backbone, coinciding with the LUMO distribution (Figure 5b).

Subsequently, we investigated the catalytic sites in the ORR process for Py-1Q. The calculations reveal that O_2 adsorption occurs preferentially at the quinoline nitrogen site with a binding energy of -1.24 eV over the pyrene ring site (-0.07 eV, Figure S22). This is consistent with the more pronounced

View Article Online
DOI: 10.1039/D6SC01713D

contribution of N into the valence band of Py-1Q (Figure S21). The next step of proton-coupled electron transfer is also favoured at the nitrogen sites (ΔG = –0.18 eV) over the pyrene site (ΔG = 0.21 eV, Figure 5c). This finding confirms that the quinoline N site provides stronger electronic coupling with adsorbed O_2 molecules, thereby facilitating electron transfer and promoting H_2O_2 formation. Taken together, the calculation results disclose that the introduced quinoline-linkage not only serves as the catalytic site for H_2O_2 production, but also provides a delocalized LUMO for charge storage, accounting for the dark photocatalysis properties. These insights would be helpful for the design of other organic energy storage systems.

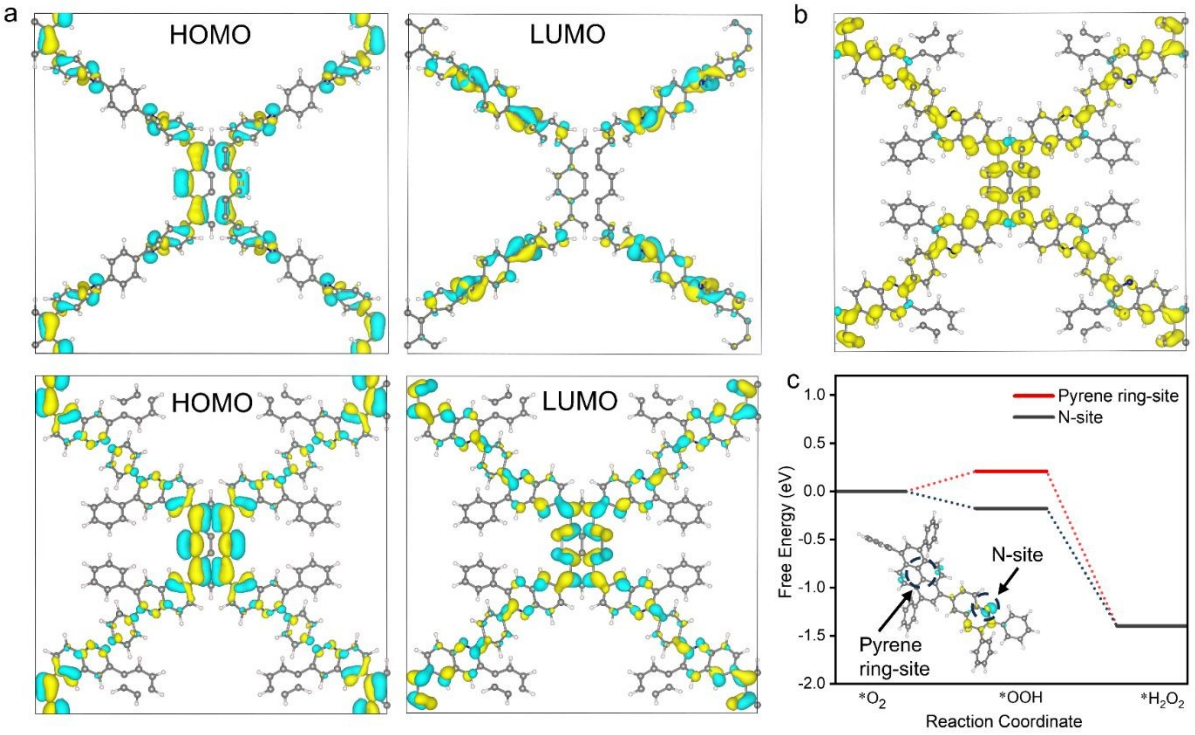

Figure 5. (a) calculated HOMO and LUMO orbital distributions of Py-1P (top) and Py-1Q (bottom). (b) Relaxed structure of Py-1Q with an additional electron per unit cell. (c) The free-energy diagrams for the two-step 1e⁻ ORR to H_2O_2 at different catalytic sites of Py-1Q.

Based on the above results, we propose a photocatalytic and dark photocatalytic H_2O_2 synthesis mechanism as illustrated in Figure 6. Upon illumination, COF undergoes photoinduced charge separation, generating electron-hole pairs (e^--h^+). The holes are quenched by H_2O, leaving H^+ and free electrons stabilized by the framework. Then, part of the photogenerated electrons is consumed to facilitate ORR, sequentially converting O_2 to $O_2^{\bullet-}$, and ultimately to H_2O_2. The rest of the stored electrons are released during the dark phase to continuously drive H_2O_2 production via ORR. In this process, electrons adjacent to the active quinoline-N site is preferentially consumed, followed by electron migration from the pyrene unit to the quinoline-N center, thereby sustaining the ORR process under dark conditions.

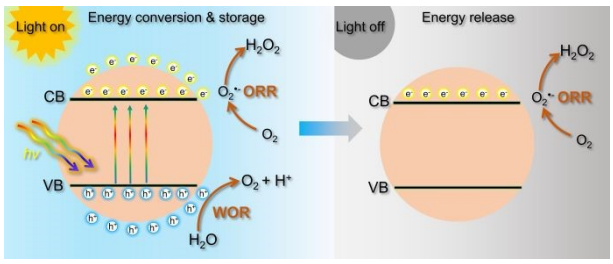

Figure 6. Proposed mechanism of photocatalytic and dark photocatalytic synthesis of H_2O_2 mediated by Py-1Q.

Conclusion

We report here a covalent organic framework as a new subset of dark photocatalytically active materials that mimics the natural photosynthetic system. The capability of both photocatalytic and dark photocatalytic properties of Py-1Q COF was demonstrated on the model reaction of oxygen reduction to H_2O_2. A H_2O_2 production rate of 1535 and 95 μmol g^{-1} h^{-1} was achieved under light and dark conditions, respectively. An electron storage capacity of 277 C g^{-1} was recorded for Py-1Q. Mechanistic studies highlight the importance of the quinoline linkage of Py-1Q COF to optimize the charge separation, transfer, and subsequent storage channels for improved photocatalysis and dark photocatalysis. These findings provide critical insights for designing next-generation artificial photosynthesis systems.

Author Contributions

T.W. contributed to the sample preparations, characterization, data analysis, conceptualization, methodology, writing and

revising the manuscript. D.C and H.W. contributed to DFT calculations and analysis, X.L. contributed to partial data test and diagram preparation. J.L., L.H., Y.S., Y.F., L.Z., S.C. and Y.N. contributed to partial data test and analysis. Y.M., J.H., T.L. led the project, providing conceptualization and supervision, writing-review and editing, and funding acquisition. All authors have given approval to the final version of the manuscript.

Conflict of Interest

The authors declare no competing financial interest.

Data Availability

The data that support the findings of this research are available in the supplementary material of this article.

Acknowledgements

This work was supported by the NSFC (Grants 22401035, 22025101, 22222103, 22173015), the Fundamental Research Funds for the Central Universities (DUT22LAB606), Liaoning Binhai Laboratory (LBLE-2023-02), and "Excellence Co-innovation Program" International Exchange Fund Project (DUTIO-ZG-202505), Guangdong Basic and Applied Basic Research Foundation (2024A1515140058), and the startup fund of Great Bay University (YJKY230010). J. H. also thanks the Guangdong Recruitment Program (2023QN10C724) for support.

Notes and references

1. J. Lv, J. Xie, A. G. A. Mohamed, X. Zhang, Y. Feng, L. Jiao, E. Zhou, D. Yuan and Y. Wang, Nat. Rev. Chem., 2022, 7, 91-105.
2. K. H. Richardson, J. J. Wright, M. Šimėnas, J. Thiemann, A. M. Esteves, G. McGuire, W. K. Myers, J. J. L. Morton, M. Hippler, M. M. Nowaczyk, G. T. Hanke and M. M. Roessler, Nat. Commun., 2021, 12, 5387.
3. R. D. Britt and D. A. Marchiori, Science, 2019, 366, 305-306.
4. D. G. Nocera, Acc. Chem. Res., 2012, 45, 767-776.
5. R. Croce and H. van Amerongen, Science, 2020, 369, eaay2058.
6. D. M. Schultz and T. P. Yoon, Science, 2014, 343, 1239176.
7. J. Schneider, M. Matsuoka, M. Takeuchi, J. Zhang, Y. Horiuchi, M. Anpo and D. W. Bahnemann, Chem. Rev., 2014, 114, 9919-9986.
8. Q. Wang and K. Domen, Chem. Rev., 2020, 120, 919-985.
9. L. Zhang and Y. Wang, Angew. Chem. Int. Ed., 2023, 62, e202219076.
10. A. Rogolino and O. Savateev, Adv. Funct. Mater., 2023, 33, 2305028. .
11. J. N. Schrauben, R. Hayoun, C. N. Valdez, M. Braten, L. Fridley and J. M. Mayer, Science, 2012, 336, 1298-1301.
12. L. Liu, W. Yang, Q. Li, S. Gao and J. K. Shang, ACS Appl. Mater. Interfaces, 2014, 6, 5629-5639.
13. Y. Takahashi and T. Tatsuma, Electrochem. Commun., 2008, 10, 1404-1407.
14. J.-J. Chen, M. D. Symes and L. Cronin, Nat. Chem., 2018, 10, 1042-1047. View Article Online DOI: 10.1039/D6SC01713D
15. Y. Pan, J. Wang, S. Chen, W. Yang, C. Ding, A. Waseem and H.-L. Jiang, Chem. Sci., 2022, 13, 6696-6703.
16. S. Wu, P. M. Stanley, S. N. Deger, M. Z. Hussain, A. Jentys and J. Warnan, Angew. Chem. Int. Ed., 2024, 63, e202406385.
17. P. M. Stanley, F. Sixt and J. Warnan, Adv. Mater., 2023, 35, 2207280.
18. S. Yao, K. Heinzerling, S. A. J. Hillman, F. Podjaski, T. He, A. García-Baldoví, Y. Baghdadi, K. Dassouki, H. García, S. Eslava, N. Steunou, S. Gonzalez-Carrero, S. Navalón, G. Mouchaham, C. Serre and J. R. Durrant, Adv. Mater., 2026, 38, e17595.
19. V. W.-h. K. Lau, D.; Kasap, H.; Podjaski, F.; Pignié, M.-C.; Reisner, E.; Jeschke, G.; Lotsch, B. V., Angew. Chem. Int. Ed., 2017, 56 (2), 510-514.
20. A. Gouder, F. Podjaski, A. Jiménez-Solano, J. Kröger, Y. Wang and B. V. Lotsch, Energy Environ. Sci., 2023, 16, 1520-1530.
21. F. Podjaski, J. Kröger and B. V. Lotsch, Adv. Mater., 2018, 30, 1705477.
22. J. Kröger, A. Jiménez‐Solano, G. Savasci, P. Rovó, I. Moudrakovski, K. Küster, H. Schlomberg, H. A. Vignolo‐González, V. Duppel, L. Grunenberg, C. B. Dayan, M. Sitti, F. Podjaski, C. Ochsenfeld and B. V. Lotsch, Adv. Energy Mater., 2021, 11, 2003016.
23. J. Lv, Y. X. Tan, J. Xie, R. Yang, M. Yu, S. Sun, M. D. Li, D. Yuan and Y. Wang, Angew. Chem. Int. Ed., 2018, 57, 12716-12720.
24. W. Wang, X. Zhang, J. Lin, L. Zhu, E. Zhou, Y. Feng, D. Yuan and Y. Wang, Angew. Chem. Int. Ed., 2022, 61, e202214816.
25. E. Zhou, X. Zhang, L. Zhu, D. Yuan and Y. Wang, Adv. Funct. Mater., 2023, 33, 2213667.
26. B. B. Rath, L. Fuchs, F. Stemmler, A. Rodríguez-Camargo, Y. Wang, M. F. X. Dorfner, J. Olbrich, J. van Slageren, F. Ortmann and B. V. Lotsch, J. Am. Chem. Soc., 2025, 147, 18492-18503.
27. K. Geng, T. He, R. Liu, S. Dalapati, K. T. Tan, Z. Li, S. Tao, Y. Gong, Q. Jiang and D. Jiang, Chem. Rev., 2020, 120, 8814-8933.
28. H. Wang, H. Wang, Z. Wang, L. Tang, G. Zeng, P. Xu, M. Chen, T. Xiong, C. Zhou, X. Li, D. Huang, Y. Zhu, Z. Wang and J. Tang, Chem. Soc. Rev., 2020, 49, 4135-4165.
29. Y. Chen and D. Jiang, Acc. Chem. Res., 2024, 57, 3182-3193.
30. B. Mishra, A. Alam, A. Chakraborty, B. Kumbhakar, S. Ghosh, P. Pachfule and A. Thomas, Adv. Mater., 2024, 37, 2413118.
31. A. Alhadhrami, A. E.-M. Ramadan and A. Fathy, Chem. Res. Chinese Universities, 2024, 40, 1068-1081.
32. N. Lu, L. Lan, Q. Gao, N. Li and X.-H. Bu, Chem. Res. Chinese Universities, 2024, 40, 675-681.
33. A. Rajca, J. Wongsriratanakul and S. Rajca, Science, 2001, 294, 1503-1505.
34. Y. Han, Z. Fei, Y.-H. Lin, J. Martin, F. Tuna, T. D. Anthopoulos and M. Heeney, npj Flex. Electron., 2018, 2, 11.
35. H. Phan, T. S. Herng, D. Wang, X. Li, W. Zeng, J. Ding, K. P. Loh, A. T. Shen Wee and J. Wu, Chem, 2019, 5, 1223-1234.
36. Y. Tan, S.-N. Hsu, H. Tahir, L. Dou, B. M. Savoie and B. W. Boudouris, J. Am. Chem. Soc., 2022, 144, 626-647.
37. O. M. Yaghi, ACS Cent. Sci., 2019, 5, 1295-1300.

View Article Online
DOI: 10.1039/D6SC01713D

38. W. Wang and Z. Huang, Chem. Res. Chinese Universities, 2025, 41, 326-332.
39. H. Hou, X. Zeng and X. Zhang, Angew. Chem. Int. Ed., 2020, 59, 17356-17376.
40. T. Freese, J. T. Meijer, B. L. Feringa and S. B. Beil, Nat. Catal., 2023, 6, 553-558.
41. A. Alam, B. Kumbhakar, A. Chakraborty, B. Mishra, S. Ghosh, A. Thomas and P. Pachfule, ACS Mater. Lett., 2024, 6, 2007-2049.
42. S. Deng, W. P. Xiong, G. X. Zhang, G. F. Wang, Y. X. Chen, W. J. Xiao, Q. K. Shi, A. Chen, H. Y. Kang, M. Cheng, Y. Liu and J. Wang, Adv. Energy Mater., 2024, 14, 2401768.
43. X. Zou, Q. Shi, M. Cheng, D. Huang, G. Zhang, W. Wang, G. Wang, H. Liu, Y. Chen, A. Chen and S. Deng, Adv. Energy Mater., 2025, 15, 2501424.
44. X. Feng, X. Wang, C. Redshaw and B. Z. Tang, Chem. Soc. Rev., 2023, 52, 6715-6753.
45. Y. Yang, S. Peng, S. Chen, F. Kang, J. Fan, H. Zhang, X. Yu, J. Li and Q. Zhang, Nanoscale Horiz., 2024, 9, 2198-2233.
46. F. Auras, L. Ascherl, A. H. Hakimioun, J. T. Margraf, F. C. Hanusch, S. Reuter, D. Bessinger, M. Döblinger, C. Hettstedt, K. Karaghiosoff, S. Herbert, P. Knochel, T. Clark and T. Bein, J. Am. Chem. Soc., 2016, 138, 16703-16710.
47. S. Ali and A. T. Khan, Org. Biomol. Chem., 2021, 19, 3255-3262.
48. P. Das, G. Chakraborty, N. Friese, J. Roeser, C. Prinz, F. Emmerling, J. Schmidt and A. Thomas, J. Am. Chem. Soc., 2024, 146, 17131-17139.
49. S. Amthor, S. Knoll, M. Heiland, L. Zedler, C. Li, D. Nauroozi, W. Tobaschus, A. K. Mengele, M. Anjass, U. S. Schubert, B. Dietzek-Ivanšić, S. Rau and C. Streb, Nat. Chem., 2022, 14, 321-327.
50. J. Kosco, S. Gonzalez‐Carrero, C. T. Howells, W. Zhang, M. Moser, R. Sheelamanthula, L. Zhao, B. Willner, T. C. Hidalgo, H. Faber, B. Purushothaman, M. Sachs, H. Cha, R. Sougrat, T. D. Anthopoulos, S. Inal, J. R. Durrant and I. McCulloch, Adv. Mater., 2022, 34, 2105007.
51. T. Huo, Q. Deng, F. Yu, G. Wang, Y. Xia, H. Li and W. Hou, ACS Appl. Mater. Interfaces, 2022, 14, 13419-13430.
52. X. Fang, B. Li, J. Huang, C. Hu, X. Yang, P. Feng, X. Dong, J. Wu, Y. Li and Y. Ding, Energy Environ. Sci., 2025, 18, 6202-6213.
53. Y. Wang, M. Yang, Y. Wang and J. Cheng, Adv. Funct. Mater., 2025, 35, 2503353.
54. Z. Chen, H. Weng, C. Chu, D. Yao, Q. Li, C. Zhang and S. Mao, Nat. Commun., 2025, 16, 6943.
55. K.-H. Xie, G.-B. Wang, F. Huang, F. Zhao, J.-L. Kan, Z.-Z. Chen, L. Cai, S.-L. Han, Y. Geng and Y.-B. Dong, Nat. Commun., 2025, 16, 3493.
56. S. Fu, X. Li, G. Wen, Y. Guo, M. A. Addicoat, M. Bonn, E. Jin, K. Müllen and H. I. Wang, Nat. Commun., 2025, 16, 2219.
57. H. Shin, D. Hong, H. Cho, H. Jang, G. Y. Kim, K. M. Song, M.-J. Choi, D. Kim and Y. S. Jung, Nat. Commun., 2024, 15, 8125.

View Article Online
DOI: 10.1039/D6SC01713D

All data supporting the findings of this study are provided in the supplementary information (SI). Additional raw data generated and analysed during the current study are available from the corresponding author upon reasonable request.